

Microstructure and Corrosion Behavior of As-Extruded Mg-1Zn-1Ca Alloy in SBF Solution Postprint

Authors: Zhang Zhongming, Yu Kai, Ren Weiwei, Ma Ying, Xu Chunjie, Hui Zengzhe

Date: 2023-03-19T00:00:00+00:00

Abstract

Mg-1Zn-1Ca (mass fraction, %) alloy was prepared through alloying, homogenization heat treatment, and forward extrusion. The corrosion behavior of the alloy in simulated body fluid (SBF) was investigated using electrochemical methods and immersion corrosion tests. The microstructure of the alloy and the morphology of the corrosion product layer were observed using OM and SEM. The phase composition of the alloy and the composition of corrosion products were analyzed using EDS attached to SEM. Fourier transform infrared absorption spectroscopy was employed for structural analysis of functional groups in the corrosion products, and the phase composition of the corrosion products was determined in combination with XRD results. The results indicate that the Mg-1Zn-1Ca alloy consists of α -Mg, Mg_2Ca , and $Ca_2Mg_6Zn_3$. After immersion in SBF solution for 72 h, the corrosion products of the Mg-1Zn-1Ca alloy were HA ($Ca_{10}(OH)_2(PO_4)_6$), $CaCO_3$, $MgCl_2$, and $Mg(OH)_2$. During the immersion corrosion process, the highly active Mg_2Ca phase acted as an anode and corroded preferentially, thereby providing a certain protective effect on the surrounding α -Mg matrix, whereas the $Ca_2Mg_6Zn_3$ phase, being the least active, accelerated the corrosion of the α -Mg matrix. The corrosion resistance of the as-extruded alloy was superior to that of the as-cast alloy.

Full Text

Microstructure of Directly Extruded Mg-1Zn-1Ca Alloy and Its Corrosion Behavior in SBF Solution

ZHANG Zhongming^{1,2}, YU Kai^{1}, REN Weiwei^{1}, MA Ying^{1}, XU Chunjie^{1}, XI Zengzhe^{2}

¹ Key Laboratory of Electrical Materials and Infiltration Technology of Shaanxi Province, School of Materials Science and Engineering, Xi'an University of Technology, Xi'an 710048

² Shaanxi Key Laboratory of Optoelectronic Functional Materials and Devices, School of Materials and Chemical Engineering, Xi'an Technological University, Xi'an 710032

Correspondent: ZHANG Zhongming, professor, Tel: (029)82312361, E-mail: zmzhang@xaut.edu.cn

Supported by: Shaanxi Provincial Science and Technology Plan Project (No.2010K10-08), Scientific Research Project of Education Department of Shaanxi Province (No.2013JK0906) and Research Project of Key Laboratory of Electrical Materials and Infiltration Technology of Shaanxi Province (No.ZSKJ201302)

Abstract

Mg-1Zn-1Ca (mass fraction, %) alloy was fabricated through alloying, homogenization heat treatment, and direct extrusion. The corrosion behavior of the alloy in simulated body fluid (SBF) was investigated using electrochemical methods and immersion testing. The microstructure and morphology of the corrosion product layer were observed using optical microscopy (OM) and scanning electron microscopy (SEM). The compositions of alloy phases and corrosion products were analyzed using energy-dispersive spectroscopy (EDS) attached to the SEM. Fourier transform infrared spectroscopy was employed to analyze the functional groups in the corrosion products, and X-ray diffraction (XRD) was used to determine the phase constituents. The results show that the Mg-1Zn-1Ca alloy consists of α -Mg, Mg_2Ca , and $Ca_2Mg_6Zn_3$ phases. After immersion in SBF for 72 h, the corrosion products are composed of HA ($Ca_{10}(OH)_2(PO_4)_6$), $CaCO_3$, $MgCl_2$, and $Mg(OH)_2$. During immersion, the highly active Mg_2Ca phase acts as the anode and corrodes preferentially, thereby providing some protection to the surrounding α -Mg matrix, while the $Ca_2Mg_6Zn_3$ phase, which has the lowest activity, accelerates corrosion of the α -Mg matrix. The corrosion resistance of the extruded alloy is superior to that of the as-cast alloy.

Key Words: Mg-1Zn-1Ca alloy, direct extrusion, microstructure, SBF solution, corrosion mechanism

Introduction

Magnesium and its alloys have emerged as promising biodegradable metallic materials for biomedical applications due to their abundant resources, low density, high strength, elastic modulus similar to human bone, excellent biocompatibility, and biodegradability within the human body. However, pure Mg and its

alloys corrode too rapidly in physiological pH environments (7.2–7.4) and physiological media containing high concentrations of aggressive ions, losing their mechanical properties before tissue healing is complete. This represents the main limitation for their clinical application.

To improve the corrosion resistance of magnesium alloys, Hradilova et al. compared the microstructural evolution of directly extruded Mg-3.6Zn and Mg-3.6Zn-0.4Ca alloys, finding that Ca addition facilitates dynamic recrystallization during direct extrusion, resulting in more uniform microstructure and improved corrosion resistance. Zhang et al. reported that direct extrusion significantly refined the grains of Mg-3Nd-0.2Zn-0.4Zr alloy and notably enhanced its corrosion resistance in simulated body fluid (SBF). Yin et al. investigated as-cast and extruded Mg-Mn-Zn alloys, demonstrating that extrusion simultaneously improves both mechanical properties and corrosion resistance. Somekawa and Mukai showed that hot extrusion of Mg-0.3Ca-1.8Zn alloy increased strength and refined grain structure. Song et al. studied the corrosion behavior of extruded AM30 magnesium alloy in salt spray and immersion environments, finding that corrosion in immersion environments occurs mainly as pitting corrosion and that the presence of Na^+ accelerates localized pitting rates.

While numerous studies have investigated the corrosion resistance of as-cast Mg and its alloys, reaching relatively consistent conclusions, reports on the corrosion resistance of extruded Mg alloys in physiological environments remain limited. Therefore, this work fabricated Mg-1Zn-1Ca alloy through conventional casting, followed by homogenization heat treatment and direct extrusion deformation to obtain an extruded alloy. Through immersion corrosion experiments in simulated body fluid (SBF), we investigated the morphology, composition, and constituent phases of the corrosion product layer on the extruded Mg-1Zn-1Ca alloy, analyzed the corrosion process, and explored the alloy's corrosion behavior.

Experimental

The experimental material was Mg-1Zn-1Ca cast magnesium alloy (mass fraction, %), prepared using pure Mg, pure Zn, and Mg-30%Ca master alloy as raw materials, melted and cast in a resistance furnace under Ar gas protection. The as-cast alloy was subjected to homogenization treatment at 330 °C for 10 h, followed by furnace cooling. Direct extrusion was performed on an XTM-108-200T four-column three-beam hydraulic press. Before extrusion, the ingot was machined into a cylinder with a diameter of 49.5 mm and length of 90 mm. The extruded rod had a diameter of 16.5 mm, corresponding to an extrusion ratio of 9:1. The extrusion temperature was 320 °C with a holding time of 10 min and an extrusion rate of 20 mm/min.

Immersion corrosion tests were conducted according to ASTM G31-1972 standard. The immersion specimens measured 15 mm in diameter and 3 mm in length. Prepared specimens were ground and polished with 2000-grit sandpa-

per, ultrasonically cleaned in acetone, dried, and immersed in SBF solution at 37 °C. The SBF solution composition is described in reference [12], and the immersion duration was 72 h. After immersion, specimens were removed, rinsed with distilled water, and dried. To observe the corrosion morphology on the alloy surface, the dried corroded specimens were immersed in boiling chromic acid solution for 3–5 min to remove surface corrosion products.

The microstructure, corrosion product morphology, and surface corrosion features were observed and analyzed using a GX71 optical microscope (OM) and a JSM-6700F scanning electron microscope (SEM). Phase compositions in the alloy and corrosion product compositions were analyzed using the energy-dispersive spectrometer (EDS) attached to the SEM, which had a secondary electron resolution of 1 nm and an EDS resolution of 133 eV. Corrosion products were gently scraped from the surface of dried corroded specimens using a glass slide. Functional group analysis of the corrosion products was performed using a Nicolet iS50 Fourier transform infrared (FT-IR) spectrometer with a wavenumber range of 400–4000 cm^{-1} and a resolution of 4 cm^{-1} . Phase constituents of the corrosion products were analyzed using an XRD-7000 X-ray diffractometer (XRD) with $\text{Cu K}\alpha$ radiation, scanning range of 20°–80°, tube current of 250 mA, and tube voltage of 40 kV.

Results and Discussion

As-Cast Alloy Microstructure

[Figure 1: see original paper] shows OM images of the as-cast Mg-1Zn-1Ca alloy. The alloy exhibits equiaxed grains approximately 200 μm in size, with second phases present at grain boundaries and within grains. A network of second phases distributed along grain boundaries and differently sized second phases within grains are visible at higher magnification.

[Figure 2: see original paper] presents OM images of the directly extruded Mg-1Zn-1Ca alloy. Comparison with [Figure 1: see original paper]b reveals that extrusion fractured the network of second phases. The longitudinal section micrograph along the extrusion direction ([Figure 2: see original paper]b) shows the formation of a fibrous structure, with second phases distributed in bands along the extrusion direction. Fine equiaxed grains smaller than 5 μm appear within the alloy, which are presumed to be dynamically recrystallized grains. This phenomenon occurs primarily because magnesium alloys have fewer slip systems, which easily generate substantial dislocation pile-ups and grain boundary distortion during plastic deformation, satisfying the conditions for recrystallization nucleation. Additionally, magnesium alloys have low stacking fault energy (78 mJ/m^2), and their high grain boundary diffusion rate enables the absorption of stacking fault energy accumulated at grain boundaries, accelerating the dynamic recrystallization process.

The XRD pattern of the as-cast Mg-1Zn-1Ca alloy is shown in [Figure 3: see original paper]. The phase constituents are identified as α -Mg, $\text{Ca}_2\text{Mg}_6\text{Zn}_3$,

and Mg_2Ca , with the α -Mg diffraction peaks showing much higher intensity than other peaks, indicating that the primary constituent phase is the α -Mg matrix.

[Figure 4: see original paper] and present SEM images of the second phases in the as-cast Mg-1Zn-1Ca alloy and their corresponding EDS analysis results. Both intragranular and grain boundary phases consist of bright and dark phases, predominantly appearing as bright phases enveloping dark phases. According to , the bright intragranular phase (Area A) contains Mg, Zn, and Ca, with Mg being the most abundant and the Zn:Ca atomic ratio approaching 3:2. Combined with the XRD results, this bright phase is identified as $\text{Ca}_2\text{Mg}_6\text{Zn}_3$. The dark intragranular phase (Area B) contains Mg and Ca with minimal Zn, and the Mg:Ca atomic ratio is close to 2:1, identifying it as Mg_2Ca . The dark grain boundary region (Area C) consists mainly of Mg and Ca with minimal Zn, confirming it as Mg_2Ca phase. The bright grain boundary phase (Area D) contains primarily Mg, Zn, and Ca, with the Zn:Ca atomic ratio approaching 3:2, identifying it as $\text{Ca}_2\text{Mg}_6\text{Zn}_3$ phase. In summary, the Mg-1Zn-1Ca alloy comprises an α -Mg matrix with second phases $\text{Ca}_2\text{Mg}_6\text{Zn}_3$ and Mg_2Ca .

According to the Mg-Zn-Ca ternary alloy phase diagram and previous studies, for Mg-xZn-xCa alloys with a Zn:Ca atomic ratio less than 1.23, a ternary eutectic reaction occurs, generating α -Mg + $\text{Ca}_2\text{Mg}_6\text{Zn}_3$ + Mg_2Ca eutectic phases. In this study, the Zn:Ca atomic ratio in Mg-1Zn-1Ca alloy is 0.61, which is less than 1.23. The solidification process proceeds as follows: when the melt temperature decreases to the liquidus temperature, primary α -Mg nucleates and precipitates. As temperature continues to drop, primary α -Mg grows, while alloying elements Zn and Ca are rejected from the solidifying α -Mg dendrites and accumulate at the liquid/solid interface, progressively enriching the Zn and Ca concentration in the residual liquid between dendrite arms and surrounding the dendrites. When temperature reaches the Mg-Ca binary eutectic temperature, the $L \rightarrow \alpha$ -Mg + Mg_2Ca eutectic reaction occurs. The α -Mg phase in the eutectic grows attached to the primary α -Mg, while the Mg_2Ca second phase precipitates in the liquid between and around the α -Mg dendrite arms; solidification is not yet complete. With further temperature decrease, the residual liquid undergoes the $L \rightarrow \alpha$ -Mg + $\text{Ca}_2\text{Mg}_6\text{Zn}_3$ + Mg_2Ca ternary eutectic reaction, completing solidification. In the ternary eutectic reaction, α -Mg and Mg_2Ca phases grow attached to the primary α -Mg and Mg_2Ca , leaving the $\text{Ca}_2\text{Mg}_6\text{Zn}_3$ phase in the interdendritic regions. The final solidification structure consists of primary α -Mg + binary eutectic (α -Mg + Mg_2Ca) + ternary eutectic (α -Mg + $\text{Ca}_2\text{Mg}_6\text{Zn}_3$ + Mg_2Ca), with the alloy composed of an α -Mg matrix and second phases Mg_2Ca and $\text{Ca}_2\text{Mg}_6\text{Zn}_3$.

To determine whether direct extrusion altered the phase composition, XRD analysis was performed on the extruded Mg-1Zn-1Ca alloy, as shown in [Figure 5: see original paper]. The phase composition remains unchanged after extrusion, still consisting of α -Mg, $\text{Ca}_2\text{Mg}_6\text{Zn}_3$, and Mg_2Ca . This is primarily because both the homogenization temperature (330 °C) and extrusion temperature (320

°C) are below the melting points of the second phases in Mg-1Zn-1Ca alloy (Mg_2Ca melts at 503 °C, $\text{Ca}_2\text{Mg}_6\text{Zn}_3$ melts at 399 °C). The effect of extrusion on the alloy's second phases is manifested mainly in their distribution morphology.

Corrosion Behavior, Morphology, and Products of Extruded Alloy After Immersion in SBF Solution

[Figure 6: see original paper] shows the polarization curves of as-cast and extruded alloys in SBF solution, with electrochemical parameters listed in . The extruded alloy exhibits a higher corrosion potential and lower corrosion current density than the as-cast alloy, indicating superior corrosion resistance.

[Figure 7: see original paper] presents SEM images of corrosion products on the surface of extruded Mg-1Zn-1Ca alloy after 72 h immersion in SBF solution, with EDS analysis results for different regions shown in . The corrosion product layer covers the entire specimen surface, appearing relatively flat in intact areas (Region A) but showing localized spalling (Region B) and cracks. Crystalline precipitates (Region C) and fluffy precipitates are observed on the corrosion product surface. The fluffy precipitates consist of densely packed needle-like crystal structures, similar to the needle-like apatite matrix of human bone collagen. This needle-like morphology exposes more surface area of the corrosion products to the SBF solution, facilitating apatite formation and promoting bone healing.

The EDS results () indicate that the main constituent elements in the corrosion product layer are Mg, O, P, C, and Ca, with O being the most abundant at approximately 60 at%, along with minor amounts of Na and Cl. The P and Ca contents in intact regions of the surface corrosion layer (Region A in [Figure 7: see original paper]a) are significantly higher than in spalled and collapsed regions (Region B in [Figure 7: see original paper]a), suggesting compositional variations at different thicknesses of the corrosion product layer. The much higher Mg content in spalled regions likely results from thinning of the corrosion product layer, exposing the substrate during EDS analysis. The EDS analysis of Region C shows elemental composition and content consistent with intact corrosion product regions.

Fourier transform infrared spectroscopy analysis of the alloy corrosion products provides information on functional group composition, aiding in identification of specific corrosion products. [Figure 8: see original paper] shows the FT-IR spectrum of Mg-1Zn-1Ca alloy corrosion products. The spectrum exhibits characteristic absorption peaks at 3697 cm^{-1} for free -OH, 3425 cm^{-1} for O-H bond stretching vibration, 1635 cm^{-1} for H_2O bending vibration, 1433 cm^{-1} for CO_3^{2-} characteristic absorption, and 1055 cm^{-1} for P-O bond characteristic absorption. Peaks at 561 and 434 cm^{-1} correspond to Mg-O bond characteristic absorptions. Combined with the EDS results (), these findings indicate that PO_4^{3-} and OH^- from the SBF solution participate in the corrosion reactions, with the corrosion products containing Ca and Mg phosphates, carbonates, and

hydroxides.

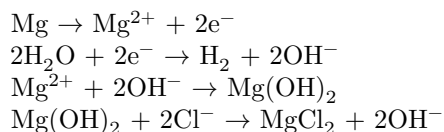
[Figure 9: see original paper] shows the XRD pattern of corrosion products on extruded Mg-1Zn-1Ca alloy after 72 h immersion in SBF solution. Combined with FT-IR and EDS results, the corrosion products after 72 h immersion are primarily HA ($\text{Ca}_{10}(\text{OH})_2(\text{PO}_4)_6$), CaCO_3 , MgCl_2 , and $\text{Mg}(\text{OH})_2$, with no toxic substances produced, indicating biocompatibility.

[Figure 10: see original paper] shows SEM images of as-cast and extruded Mg-1Zn-1Ca alloy surfaces after removal of corrosion products in boiling chromic acid. The as-cast alloy surface exhibits severe corrosion with corrosion pits of varying sizes and depths, showing a tendency for lateral interconnection and longitudinal penetration into the alloy interior. In contrast, the extruded alloy shows less severe surface corrosion, with more uniform pit depths and no tendency for deep penetration into the alloy interior, while retaining large areas of relatively intact matrix. Some second phases remain in these less-corroded regions, and EDS analysis reveals their composition as O, Mg, Ca, and Zn with mass fractions of 1.65%, 88.23%, 0.49%, and 9.63%, respectively. After 72 h immersion, Ca in the alloy second phases has been largely corroded away, leaving only oxides of Mg and Zn.

Discussion

Formation of Corrosion Products

The analysis demonstrates that the corrosion products of extruded Mg-1Zn-1Ca alloy are primarily HA ($\text{Ca}_{10}(\text{OH})_2(\text{PO}_4)_6$), CaCO_3 , MgCl_2 , and $\text{Mg}(\text{OH})_2$. Due to the reactive nature of magnesium alloys, the following reactions occur in Cl^- -containing aqueous solutions, forming MgCl_2 and $\text{Mg}(\text{OH})_2$:



When Mg-1Zn-1Ca alloy is immersed in SBF solution, rapid reactions occur, forming $\text{Mg}(\text{OH})_2$ and establishing a corrosion product layer on the specimen surface. As immersion proceeds, the corrosion product layer gradually thickens. However, the $\text{Mg}(\text{OH})_2$ layer is not dense enough to provide adequate protection. According to reaction (4), aggressive Cl^- ions in the solution react with $\text{Mg}(\text{OH})_2$ to form soluble MgCl_2 , further compromising the protective function of the corrosion product layer.

Zhang et al. reported that when solutions contain PO_4^{3-} and Ca^{2+} , HA ($\text{Ca}_{10}(\text{OH})_2(\text{PO}_4)_6$) readily nucleates and grows on Mg surfaces due to supersaturation conditions and high pH. HA ($\text{Ca}_{10}(\text{OH})_2(\text{PO}_4)_6$) exhibits excellent biocompatibility, bioactivity, and biodegradability, making it an ideal material for human hard tissue repair and replacement. The formation of another corrosion product, CaCO_3 , can be described by the following reaction:



The HCO_3^- in reaction (5) originates partly from the SBF solution itself and partly from dissolution of atmospheric CO_2 in the solution. The Ca^{2+} comes from both the SBF solution and dissolution of the Mg_2Ca phase, while OH^- is a byproduct of Mg dissolution. As corrosion progresses, continuous supply of Ca^{2+} , HCO_3^- , and OH^- leads to precipitation of CaCO_3 on the magnesium alloy surface.

Corrosion Behavior

The standard electrode potential of metals serves as a criterion for judging corrosion resistance, with lower potentials indicating stronger oxidation tendency and greater susceptibility to corrosion. The second phases in Mg-1Zn-1Ca alloy are $\text{Ca}_2\text{Mg}_6\text{Zn}_3$ and Mg_2Ca . Du et al. reported that the three phases in Mg-1Zn-1Ca alloy can be ordered by potential as: $\text{Ca}_2\text{Mg}_6\text{Zn}_3 > \alpha\text{-Mg} > \text{Mg}_2\text{Ca}$, indicating that Mg_2Ca is more active than both $\text{Ca}_2\text{Mg}_6\text{Zn}_3$ and $\alpha\text{-Mg}$ phases, while $\text{Ca}_2\text{Mg}_6\text{Zn}_3$ is less active than the $\alpha\text{-Mg}$ phase.

Kirkland et al. demonstrated that the high activity of Mg_2Ca is attributed to its lattice parameters. Both Mg_2Ca and $\alpha\text{-Mg}$ have hexagonal crystal structures, but the lattice parameters of Mg_2Ca are approximately twice those of $\alpha\text{-Mg}$. This results in a Pilling-Bedworth ratio (PBR, the ratio of oxide volume to consumed metal volume) for Mg_2Ca that is smaller than that of $\alpha\text{-Mg}$, indicating that neither surface film provides adequate substrate protection, with Mg_2Ca being more active.

During corrosion of both as-cast and extruded Mg-1Zn-1Ca alloys, the second phases $\text{Ca}_2\text{Mg}_6\text{Zn}_3$ and Mg_2Ca form galvanic couples, where the Mg_2Ca phase acts as the anode and corrodes preferentially, while $\text{Ca}_2\text{Mg}_6\text{Zn}_3$ acts as the cathode with H_2 evolution. Simultaneously, dissolution of the Mg_2Ca phase increases the Ca^{2+} concentration, facilitating precipitation of HA ($\text{Ca}_{10}(\text{OH})_2(\text{PO}_4)_6$) and CaCO_3 . After complete dissolution of Mg_2Ca , the $\text{Ca}_2\text{Mg}_6\text{Zn}_3$ phase and surrounding $\alpha\text{-Mg}$ matrix form a galvanic couple, where $\alpha\text{-Mg}$ acts as the anode and corrodes while $\text{Ca}_2\text{Mg}_6\text{Zn}_3$ acts as the cathode with H_2 evolution. When corrosion progresses to a certain extent, severe corrosion of $\alpha\text{-Mg}$ around $\text{Ca}_2\text{Mg}_6\text{Zn}_3$ phases causes some $\text{Ca}_2\text{Mg}_6\text{Zn}_3$ phases to lose support and detach, forming corrosion pits.

The difference in corrosion resistance between as-cast and extruded alloys arises from significant grain refinement, reduced solute segregation, more uniform dispersion of second phases, and improved casting defects that cause non-uniform corrosion after extrusion. The overall microstructure becomes more uniform and dense, reducing the tendency for galvanic corrosion and localized corrosion, thereby making the alloy corrosion more uniform.

Conclusions

1. The Mg-1Zn-1Ca alloy consists of an α -Mg matrix with second phases Mg_2Ca and $\text{Ca}_2\text{Mg}_6\text{Zn}_3$.
2. After 72 h immersion in SBF solution, the corrosion products of extruded Mg-1Zn-1Ca alloy are composed of HA ($\text{Ca}_{10}(\text{OH})_2(\text{PO}_4)_6$), CaCO_3 , MgCl_2 , and $\text{Mg}(\text{OH})_2$, with no toxic substances produced, indicating biocompatibility. Some corrosion product layers exhibit densely packed needle-like crystal structures that promote bone healing.
3. During immersion corrosion, the highly active Mg_2Ca phase acts as the anode and corrodes preferentially, providing some protection to the surrounding α -Mg matrix, while the $\text{Ca}_2\text{Mg}_6\text{Zn}_3$ phase, having the lowest activity, accelerates corrosion of the α -Mg matrix.
4. The corrosion resistance of extruded Mg-1Zn-1Ca alloy in SBF solution is superior to that of the as-cast alloy.

References

- [1] Mark P S, Alexis M P. *Biomaterials*, 2006; 27: 1728
- [2] Li K K, Wang B, Yan B. *Corros Sci Protect Technol*, 2012; 24: 181
- [3] Moravej M, Mantovani D. *Int J Mol Sci*, 2011; 12: 4250
- [4] Wen Z, Wu C, Dai C. *J Alloys Compd*, 2009; 488: 392
- [5] Xin Y C, Huo K F, Tao H, Tang G Y, Chu P K. *Acta Biomater*, 2008; 4: 2008
- [6] Hradilova M, Montheillet F, Frackiewicz A, Desrayaud C, Lejcek P. *Mater Sci Eng*, 2013; A580: 217
- [7] Zhang X, Yuan G, Mao L, Niu J, Fu P, Ding W. *Biomaterials*, 2012; 7: 77
- [8] Yin D S, Zhang E L, Zeng S Y. *Trans Mater Heat Treat*, 2009; 114: 118
- [9] Somekawa H, Mukai T. *Mater Sci Eng*, 2007; A459: 366
- [10] Song W W, Martin H J, Hicks A, Seely D, Walton C A, Lawrimore II W B, Wang P T, Horstemeyer M F. *Corros Sci*, 2014; 78: 313
- [11] Bakhsheshi-Rad H R, Abdul-kadir M R, Idris M H, Farahany S. *Corros Sci*, 2012; 64: 184
- [12] Kokubo T, Takadama H. *Biomaterials*, 2006; 27: 2907
- [13] Mao P L, Yu J C, Liu Z. *Chin Trans Nonferrous Met Soc*, 2013; 23: 889
- [14] Wang Q, Wang J F, Huang S. *J Mater Eng Perform*, 2013; (11): 57
- [15] Liu C M, Zhu X R, Zhou H T. *Phase Diagrams for Magnesium Alloys*. Changsha: Central South University Press, 2006: 1
- [16] Wasiur-Rahman S, Medraj M. *Intermetallics*, 2009; 17: 847
- [17] Farahany S, Bakhsheshi-Rad H R, Idris M H, Abdul-kadir M R, Lotfabadi A F, Ourdjini A. *Thermochim Acta*, 2012; 527: 180
- [18] Meng E C, Guan S K, Wang H X, Wang L G, Zhu S J, Hu J H, Ren C X, Gao J H, Feng Y S. *Appl Surf Sci*, 2011; 257: 4811
- [19] Zhang X, Liang M J, Liao H H, Bai P K, Huang S. *Hot Working Technol*, 2014; 43(8): 9

- [20] Fang S J, Liu Y H, Dong G D. Corros Sci Protect Technol, 2008; 20: 100
- [21] Li Z J, Gu X A, Lou S Q. Biomaterials, 2008; 29: 1329
- [22] Zhang S X, Zhang X N, Zhao C L, Li J N, Song Y, Xie C Y, Tao H R, Zhang Y, He Y H, Jiang Y, Bian Y J. Acta Biomater, 2010; 6: 626
- [23] Du H, Wei Z J, Liu X W, Zhang E. Mater Chem Phys, 2011; 125: 1
- [24] Bakhsheshi-Rad H R, Idris M H, Abdul-Kadir M R, Ourdjini A, Medraj M, Daroonparvar M, Hamzah E. Mater Des, 2014; 53: 283
- [25] Kirkland N T, Birbilis N, Walker J, Woodfield T, Dias G J, Staiger M P. Biomed Mater Res, 2010; 95B: 91

Note: Figure translations are in progress. See original paper for figures.

Source: ChinaXiv — Machine translation. Verify with original.